This method could also be adopted to determine the reversal wavelengths for $q_{11}-q_{12}$.

APPENDIX

$$E'=\frac{4(C_{11}-C_{12})(C_{11}+2C_{12})C_{44}}{C}$$

$$\sigma_{x'}=\frac{2C_{11}C_{44}-(C_{11}-C_{12})(C_{11}+2C_{12})}{C}$$

$$\sigma_{y'}=\frac{2C_{12}C_{44}}{C},$$

where

$$C=2C_{11}C_{44}+(C_{11}-C_{12})(C_{11}+2C_{12}).$$

References

BANSIGIR, K. G. & IYENGAR, K. S. (1961*a*). *Acta Cryst.* **14**, 670–674.

BANSIGIR, K. G. & IYENGAR, K. S. (1961*b*). *Acta Cryst.* **14**, 727–732.

BRAYBORN, J. E. H. (1953). *Proc. Phys. Soc.* B**66**, 61–63.

FRÖHLICH, H. (1949). *Theory of Dielectrics*. Oxford: Clarendon Press.

HAVELOCK, T. H. (1908). *Proc. Roy. Soc.* A**80**, 28–44.

LAIHO, R. & KORPELA, A. (1968). *Ann. Acad. Sci. Fenn. A*, **6**, 272–276.

MUELLER, H. (1935). *Physics*, **6**, 179.

POCKELS, F. (1906). *Lehrbuch der Kristalloptik*. Berlin: Teubner.

RAHMAN, A. & IYENGAR, K. S. (1970). *Acta Cryst.* A**26**, 128–133.

Acta Cryst. (1973). A**29**, 160

Derivation and Experimental Verification of the Normalized Resolution Function for Inelastic Neutron Scattering*

BY N. J. CHESSER†‡

Physics Department, SUNY at Stony Brook, Stony Brook, New York 11790 *and Brookhaven National Laboratory, Upton, New York* 11973, *U.S.A.*

AND J. D. AXE

Brookhaven National Laboratory, Upton, New York 11973, *U.S.A.*

(*Received* 14 *June* 1972; *accepted* 14 *September* 1972)

Based upon the work of Cooper & Nathans, an expression for the normalized resolution function of a triple-axis neutron spectrometer is derived and tested experimentally. The formalism is extended to show the explicit dependence of the integrated intensity of a sharp excitation spectrum on all of the relevant instrumental parameters. Extensive measurements of the integrated intensities of phonons in copper have been carried out for a wide range of all adjustable parameters. The experimentally determined intensities are found to be in good agreement with the calculated values.

1. Introduction

Resolution effects in triple-axis neutron spectrometers were first considered by Caglioti, Paoletti & Ricci (1958) and Collins (1963). These authors considered the effect of horizontal collimations and mosaic spreads for special arrangements of relaxed collimations. Stedman (1968) and Bjerrum Møller & Nielsen (1970) derived expressions for the dependence of the intensity on the horizontal collimation, mosaic spread of the monochromator and analyzer crystals and Bragg angles of those crystals. Expressions for the width of an inelastic peak were derived by Stedman & Nilsson (1966), Cooper & Nathans (1967) and Nielsen & Bjerrum Møller (1969). Though derived by different methods, the expressions for the peak width are in mutual agreement. None of these authors, however, is concerned with the correct normalization of the resolution function since they were interested in line shapes rather than in accurate measurements of scattering intensities.

Although an essentially correct formulation of the resolution-function normalization has existed in our laboratory for several years [see for example Samuelsen, Hutchings & Shirane (1970)], in the course of a study of phonon intensities in zinc we felt it necessary to formalize the derivation and to test experimentally the salient features of the results. To this end, we have extended the resolution-function calculations of Cooper & Nathans (1967)* to give a closed analytic expression for the normalized resolution function of a triple-axis spectrometer. This result is used to derive the inte-

* Work performed under the auspices of the U. S. Atomic Energy Commission.

† Work supported by the U. S. Atomic Energy Commission Grant No. AT(30-1)-4084 Mod. 1.

‡ Present address: Ames Laboratory–USAEC and Department of Physics, Iowa State University, Ames, Iowa 50010.

* See Appendix.

grated intensity for a constant Q scan of a sharp excitation, *i.e.* one with scattering law of the form $S(Q,\omega)\propto\delta(\omega-\omega(q))$. These expressions are in substantial agreement with those of Tucciarone, Lau, Corliss, Delapalme & Hastings (1971).* We also agree with the formulation of Dorner (1972) derived by a geometric method.

A series of measurements of integrated phonon intensities has been carried out using a single crystal of copper. The parameters of our formulation, $Q,k_F,k_I,\hbar\omega$ and horizontal and vertical collimations, were varied over as wide a range as was readily available. To within experimental error, the measured integrated intensities agree with the calculated values.

2. Derivation of the normalization R_0

It has been shown by Cooper & Nathans (1967) that for energy transfer $\hbar\omega=(\hbar^2/2m)(k_i^2-k_f^2)$ and wave vector transfer $\mathbf{Q}=\mathbf{k}_i-\mathbf{k}_f$, the resolution function of a triple-axis spectrometer can be written

$$R(\mathbf{Q}_0+\Delta\mathbf{Q},\,\omega_0+\Delta\omega) = R_0\exp\{-\tfrac{1}{2}\sum_{k=1}^{4}\sum_{l=1}^{4}M_{kl}X_kX_l\}\,, \quad (1)$$

where X_1,X_2,X_3 are the Cartesian components of $\Delta\mathbf{Q}$ and X_4 is $\Delta\omega$. X_1 is chosen parallel to $-\mathbf{Q}_0$, X_3 is vertical (perpendicular to the scattering plane). $\mathbf{Q}_0$ and ω_0 are the nominal setting of the instrument as defined by the most probable wave vectors $\mathbf{k}_I$ and $\mathbf{k}_F$. R_0 depends on $\mathbf{Q}_0$ and ω_0 as well as on the instrumental parameters.

There are nine factors included in R_0 which arise from different steps in the derivation of (1). Written explicitly, these are

$$R_0=\varphi\,.\,\varepsilon_D\,.\,P_{0M}\,.\,P_{0A}\,.\,N_M\,.\,N_A\,.\,J\,.\,R_{0x}\,.\,R_{0z}$$

where

$$\begin{aligned}
P_{0M}&=(2\pi)^{1/2}\left(\frac{1}{\beta_0^2}+\frac{1}{(2\eta_M'\sin\theta_M)^2}\right)^{-1/2}\\
P_{0A}&=(2\pi)^{1/2}\left(\frac{1}{\beta_3^2}+\frac{1}{(2\eta_A'\sin\theta_A)^2}\right)^{-1/2}\\
N_M&=(2\pi)^{-1/2}\left(\frac{P_M}{2\eta_M'\sin\theta_M}\right) \qquad (2)\\
N_A&=(2\pi)^{-1/2}\left(\frac{P_A}{2\eta_A'\sin\theta_A}\right)\\
J&=m/(\hbar k_I^2k_F^3\sin 2\theta_S)\\
R_{0x}&=(2\pi)^{1/2}(A')^{-1/2}\\
R_{0z}&=(2\pi)^{1/2}(a_{11}^2+a_{12}^2)^{-1/2}\,.
\end{aligned}$$

The notation is primarily that of Cooper & Nathans (1967). β_i and α_i are the vertical and horizontal collimations respectively where $i=0,1,2,3$ refers to the inpile, monochromator-to-sample, sample-to-analyzer and analyzer-to-detector collimators as shown in Fig. 1. η_j and η_j' are the horizontal and vertical mosaic spreads of crystal j while P_j is the reflectivity of that crystal as defined below. $j=M$ or A refers to the monochromator or analyzer crystal. ε_D is the efficiency of the detector. φ is the flux of the reactor defined such that $\varphi dk_I d\Omega$ is the flux in a volume dk_I about k_I and $d\Omega$ about Ω. For example, if the reactor follows a Maxwellian distribution, φ is given by

$$\varphi=\frac{\varphi_0}{2\pi}(k_I^3/k_T^4)\exp(-k_I^2/k_T^2) \qquad (3)$$

where φ_0 is the total flux of the reactor and where k_T is such that $\hbar^2k_T^2/(2m)=k_BT$, T is the temperature of the moderator, k_B is the Boltzmann constant.

We assume that the flux in the detector is the product of the flux of neutrons incident on the spectrometer and the normalized probability of passage through the spectrometer. The basic steps in the derivation of equation (1) are:

(*A*) Define the probability that a neutron of given wave vector $\mathbf{k}$ will pass through each component of the spectrometer in terms of the variation in the magnitude of $\mathbf{k}$ and the horizontal and vertical divergence angles. Assuming a sample of unit cross section, the probability of passage through the spectrometer is the product of the probabilities of the components.

(*B*) Transform to variables x_1,y_1,z_1 and x_2,y_2,z_2 the

* See Appendix.

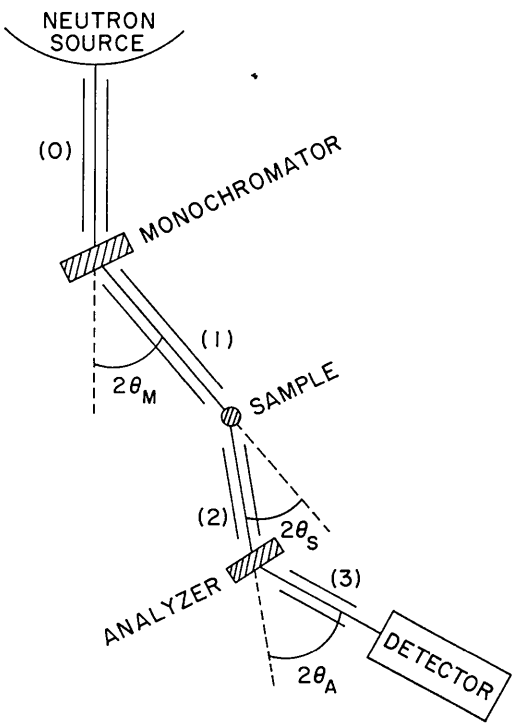

Fig. 1. Schematic representation of the triple-axis neutron spectrometer.

Cartesian components of $\Delta\mathbf{k}_I$ and $\Delta\mathbf{k}_F$ respectively.

(*C*) Transform to variables $X_1, X_2, X_3, X_4, x_1, z_1$ as defined above.

(*D*) Integrate over x_1.

(*E*) Integrate over z_1.

It should be noted that the probabilities as defined in step *A* determine the form of the flux (per unit solid angle per unit incident wave vector) given above. The, cross section to be used to represent the sample must be a partial cross section with respect to wave vector and solid angle. We note that the choice of variables in step *B* is arbitrary in that each variable is eliminated either by a successive transformation (step *C*) or by integration (steps *D* and *E*).

The factor J given in (2) is just the Jacobian of the transformations in steps *B* and *C*. R_{0_x} is the result of the integration over x_1 while R_{0_z} is the result of that over z_1. In Cooper & Nathans (1967) there is defined a P_{0_M} arising from integration over the vertical divergence angle before the monochromator. P_{0_A} is the corresponding term for the angle after the analyzer.

The probability of passage of a neutron through a crystal j as a function of horizontal and vertical divergence angles, δ_H and δ_V, is given by

$$P_j(\delta_H\delta_V) = N_j \exp\left\{-\tfrac{1}{2}\left(\frac{\delta_H^2}{\eta_j^2} + \frac{\delta_V^2}{(2\eta_j' \sin\theta_j)^2}\right)\right\}. \quad (4)$$

The total probability of passage is given by

$$\int\int P_j(\delta_H\delta_V)\mathrm{d}\delta_H\mathrm{d}\delta_V = P_j \int \exp\left\{-\tfrac{1}{2}\frac{\delta_H^2}{\eta_j^2}\right\}\mathrm{d}\delta_H . \quad (5)$$

This relation defines N_j as given above.

Combining terms and simplifying gives the normalization R_0,

$$R_0 = 2\pi\varphi\varepsilon_D P_M P_A \frac{m}{\hbar k_I^2 k_F^3 \sin 2\theta_s}\{A'(a_{11}^2 + a_{12}^2)\}^{-1/2} \times \left\{\left(\frac{\beta_0^2}{\beta_0^2 + (2\eta_M' \sin\theta_M)^2}\right)\left(\frac{\beta_3^2}{\beta_3^2 + (2\eta_A' \sin\theta_A)^2}\right)\right\}^{1/2}. \quad (6)$$

Werner & Pynn (1971) have considered the spectrometer resolution with no collimation before the monochromator or after the analyzer. Making allowances for different definitions, their results can be shown to follow from equation (6). Equation (6) also agrees with the normalization derived by Tucciarone, Lau, Corliss, Delapalme & Hastings (1971) if one includes a correction brought to the attention of these authors by B. Dorner and one of the present authors (NJC). Their note 25 mentions this correction but should read, 'P_0... must be multiplied by the factor $1/(2\pi\eta_m'\eta_A')$.'

3. Intensities for a planar dispersion surface

The measured intensity I is given by the convolution of the resolution function with the scattering cross section σ,

$$I(\mathbf{Q}_0,\omega_0) = \int\int\int\int R(\mathbf{Q}_0 + \Delta\mathbf{Q}, \omega_0 + \Delta\omega)\sigma(\mathbf{Q}_0 + \Delta\mathbf{Q}, \omega_0 + \Delta\omega)\mathrm{d}(\Delta\mathbf{Q})\mathrm{d}(\Delta\omega) . \quad (7)$$

As was stated above, this cross section must be written in terms of $\mathrm{d}\Delta k_F \mathrm{d}\Omega_F$, thus

$$\sigma(\mathbf{Q}_0 + \Delta\mathbf{Q}, \omega_0 + \Delta\omega) = \frac{\mathrm{d}^2\sigma}{\mathrm{d}\Delta k_F \mathrm{d}\Omega_F} = \frac{\hbar k_F}{m}\frac{\mathrm{d}^2\sigma}{\mathrm{d}\omega\mathrm{d}\Omega} . \quad (8)$$

Although the integration in (7) can always be performed numerically, it can be carried out analytically if we assume that, as a first approximation, the dispersion surface is planar. If this planar dispersion surface is characterized by a slope $C = -\mathrm{grad}_q\omega(q)$, then the cross section contains a delta function which restricts X_4 to the plane $X_4 = W - C_1X_1 - C_2X_2 - C_3X_3$. This restriction is pictured in Q,ω space in Fig. 2. The assumption of a planar dispersion surface is approximately valid locally in many cases since it is only necessary that the assumption hold over that volume where the resolution function is appreciable. The cross section can now be written

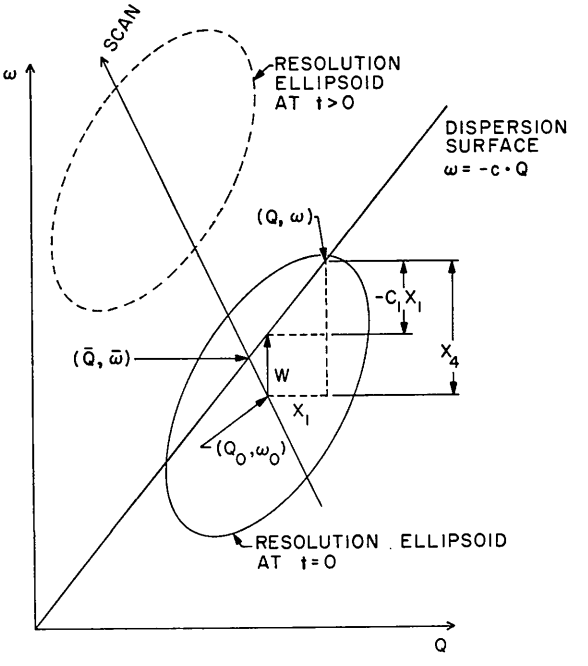

Fig. 2. A cross section of the resolution ellipsoid in Q_1,ω space. The scan is defined as the path of Q_0,ω_0, the nominal setting of the spectrometer. $\bar{Q}$, $\bar{\omega}$ is that point where the scan crosses the dispersion surface. Only those values of $(\mathbf{Q},\omega) = (\mathbf{Q}_0 + \mathbf{X}_1 + \mathbf{X}_2 + \mathbf{X}_3, \omega_0 + X_4)$ which satisfy the delta function $\delta(X_4 - W + C_1X_1 + C_2X_2 + C_3X_3)$ will contribute to the intensity. The dashed curve shows the resolution ellipsoid at a later point in the scan.

$$\sigma(\mathbf{Q}_0+\Delta\mathbf{Q},\omega_0+\Delta\omega)=\frac{\hbar k_F^2}{mk_I}\hat{S}(Q,\omega)$$
$$\times\delta(X_4-W+C_1X_1+C_2X_2+C_3X_3)$$
$$=\frac{\hbar k_F^2}{mk_I}S(Q,\omega)\,. \tag{9}$$

It is often permissible to assume that $\hat{S}(Q,\omega)$ is constant over that volume in Q,ω space where the resolution function is appreciable. This approximation is generally acceptable except near $q=0$ (and perhaps near other Van Hove singularities) where the properties of the excitations may vary rapidly with either the magnitude or direction of q, and the curvature of the dispersion surface becomes important. This assumption allows us to take $\hat{S}(Q,\omega)$ outside the integration. If we define $(\bar{Q},\bar{\omega})$ as the point at which the center of the scan crosses the dispersion surface then from Fig. 2 we see that at that point $W=0$ and the intensity is maximum. The intensity I is given by the product of $S(\bar{Q},\bar{\omega})$ and the integral of the resolution function over the delta function in equation (9). Letting $m=\hbar=1$, the intensity is found to be a Gaussian with full width at half maximum (FWHM) equal to $(21n2)^{1/2}\Delta$. That is

$$I=I(\bar{Q},\bar{\omega})\exp\{-\tfrac{1}{2}W^2/\Delta^2\}$$

where

$$\Delta^2=S_1/S_2\,. \tag{10}$$

Care must be taken in comparison of this expression with experimental data in that such comparison is straightforward only if the data are treated as a function of the independent variable W. For a constant Q scan, W coincides with the energy and no conversion is necessary. The necessary conversion for other types of scans is discussed in § 4(*D*). The peak intensity, $I(\bar{Q},\bar{\omega})$, is proportional to R_0 and $S(\bar{Q},\bar{\omega})$ and hence is a slowly varying function of W. S_1 and S_2 are given in terms of the M_{kl} defined in Cooper & Nathans (1967) by

$$S_2=M_{33}T_2$$
$$S_1=C_3^2T_2+M_{33}\{M_{11}M_{22}-M_{12}^2-(C_1M_{24}-C_2M_{14})^2$$
$$+2M_{24}(C_1M_{12}-C_2M_{11})+2M_{14}(C_2M_{12}-C_1M_{22})$$
$$+M_{44}(C_1^2M_{22}+C_2^2M_{11}-2C_1C_2M_{12})\} \tag{11}$$

where

$$T_2=M_{11}M_{22}M_{44}-M_{11}M_{24}^2-M_{22}M_{14}^2-M_{44}M_{12}^2$$
$$+2M_{12}M_{14}M_{24}\,.$$

We note that if the sample mosaic spread is large then M_{kl} should be replaced by M'_{kl} as defined by Werner & Pynn (1971).

If we consider the M_{kl} to define the elements of a 4×4 matrix M then S_2 is just the determinant of that matrix. T_2 is the determinant of the 3×3 submatrix obtained from M by omitting the vertical elements, *i.e.* of the cofactor of M_{33}.

We note that the only dependence on the slope of the dispersion curve in the vertical direction occurs as C_3^2 in S_1. Thus the width of the peak depends only on the magnitude and not on the sign of the vertical slope. In the limit of $C_3=0$, Δ^{-2} becomes G_3^2 as defined by Cooper & Nathans (1967). In the same limit S_1^{-1} becomes G_1G_2/M_{33}.

The integrated intensity $\mathscr{I}$ is given by

$$\mathscr{I}=\int I(\bar{Q},\bar{\omega})\exp\{-\tfrac{1}{2}W^2/\Delta^2\}\,\mathrm{d}W$$
$$=I(\bar{Q},\bar{\omega})\sqrt{2\pi}\,\Delta=R_0\left[\frac{k_F^2}{k_I}\right]S(\bar{Q},\bar{\omega})\,V \tag{12}$$

where

$$V=(2\pi)^2(S_1^{-1}\Delta^2)^{1/2}=(2\pi)^2(S_2)^{-1/2}\,.$$

V is the volume of the resolution ellipsoid defined as the locus of points where the resolution is one half that at the maximum point. V is independent of the slope of the dispersion surface. Hence, as would be expected, the integrated intensity of a phonon peak is independent of the slope of the dispersion surface.

Substituting for R_0 and V in the expression for the integrated intensity we find

$$\mathscr{I}=(2\pi)^3S(\bar{Q},\bar{\omega})\varphi\varepsilon_DP_MP_AF_{VI}F_{VF}F_{HI}F_{HF}$$
$$\times\frac{k_F^3}{\tan\theta_A}\frac{1}{\tan\theta_M}$$

where

$$F_{HI}=\alpha_0\alpha_1\eta_M(\alpha_0^2+\alpha_1^2+4\eta_M^2)^{-1/2}$$
$$F_{HF}=\alpha_2\alpha_3\eta_A(\alpha_2^2+\alpha_3^2+4\eta_A^2)^{-1/2}$$
$$F_{VI}=\beta_0\beta_1(\beta_0^2+\beta_1^2+[2\eta'_M\sin\theta_M]^2)^{-1/2}$$
$$F_{VF}=\beta_2\beta_3(\beta_2^2+\beta_3^2+[2\eta'_A\sin\theta_A]^2)^{-1/2}\,. \tag{13}$$

F_{VI} and F_{VF} contain all dependence on vertical terms before and after the sample respectively. It should be noted that the only dependence on Q is that contained in $S(\bar{Q},\bar{\omega})$. Thus intensity data for one value of q and ω and different values of Q can be analyzed without concern for resolution. As was the case with equation (10) this expression can be compared directly with experimental data only if the data are treated as a function of the independent variable W.

This expression for the integrated intensity is in complete agreement with that of Tucciarone, Lau, Corliss, Delapalme & Hastings (1971) subject to the correction mentioned previously.

4. Special cases

(*A*) In many instances, particularly for diffuse elastic scattering as well as for phonons on an optic branch or near a zone boundary, the slope of the dispersion curve approaches zero. This limit greatly simplifies the expressions given above. Since the integral intensity is independent of slope, calculation of Δ^2 in the limit of

zero slope is sufficient to determine both the width and the peak height in that limit through knowledge of the integrated intensity.

In the limit of $C_i=0$ the width becomes

$$\Delta^2=k_F^4B_F+k_I^4B_I$$

where

$$B_F=\left(\frac{1}{\eta_A^2}+\frac{1}{\alpha_2^2}+\frac{1}{\alpha_3^2}\right)F_{HF}^2/\tan^2\theta_A \qquad (14)$$

$$B_I=\left(\frac{1}{\eta_M^2}+\frac{1}{\alpha_0^2}+\frac{1}{\alpha_1^2}\right)F_{HI}^2/\tan^2\theta_M\,.$$

(*B*) With the usual arrangement of tight horizontal collimation and relaxed vertical collimation, the vertical terms can be simplified by an approximation. In the limit that $\beta_i\gg\eta_j'$ for all elements on the same side of the sample, the vertical terms become $F_{V_I}=\beta$ and $F_{V_F}=\beta'$ where β and β' are effective collimations given by $\beta^{-2}=\beta_0^{-2}+\beta_1^{-2}$ and $\beta'^{-2}=\beta_2^{-2}+\beta_3^{-2}$.

(*C*) In most experiments, a monitor is placed just before the sample and all measurements are made as a function of a constant monitor count. In this case, intensities as defined above must be modified by division by the integrated intensity at the monitor. This quantity is found by dropping all those terms in $\mathscr{I}$ arising from elements after the monitor. Dropping factors of 2π, this is just

$$\mathscr{I}(\text{monitor})=\varphi P_M F_{H_I}F_{V_I}\varepsilon_M k_I/\tan\theta_M\,. \qquad (15)$$

ε_M is the efficiency of the monitor. This results in a measured integrated intensity,

$$\mathscr{I}_M=\;S(\bar{Q},\bar{\omega})\,[\varepsilon_D/\varepsilon_M]P_AF_{V_F}F_{H_F}\frac{1}{k_I}\,[k_F^3/\tan\theta_A]\,. \qquad (16)$$

The width will, of course, be unaffected by insertion of the monitor.

(*D*) As was pointed out earlier, the expressions derived here treat W as the independent variable and comparison with data is straightforward only if the data are treated as a function of that variable. Examination of Fig. 2 reveals that for a constant Q scan, W is just the energy, the usual choice of variable. Further examination reveals that for any other type of scan, some conversion must be made since W will also depend on Q. This conversion is discussed in detail by Sears & Dolling (1972). For a constant energy scan, W differs from Q, the usual choice of independent variable by a factor of C, the slope of the dispersion curve. Thus the width as a function of Q will be $\Delta'=\Delta/|C|$ and the integrated intensity must be converted by the same factor.

5. Experimental verification

In the harmonic approximation, $S(Q,\omega)$ for a crystal with one atom per unit cell can be written

$$S(Q,\omega)=C_0(N_j+\tfrac{1}{2}\mp\tfrac{1}{2})e^{-2w(Q)}\,|\mathbf{Q}\,.\,\mathbf{e}_j|^2\,(\hbar\omega_j)^{-1}\times\delta(\omega\pm\omega_j(q))\delta(\mathbf{Q}-\mathbf{G}-\mathbf{q}) \qquad (17)$$

where $\mathbf{G}$ is a reciprocal lattice vector, $\mathbf{e}_j$ is the phonon polarization vector associated with the jth branch of the dispersion curve, ω_j is the corresponding frequency, $W(Q)$ is the Debye–Waller factor, N_j is the Bose–Einstein occupation number $(\exp[\hbar\omega_j/k_BT]-1)^{-1}$, C_0 is a constant. The upper sign refers to phonon annihilation, the lower to phonon creation.

Substituting this expression into equation (16) for the measured integrated intensity we find

$$\mathscr{I}_M=C_0F_\omega F_Q F_{k_I}F_{k_F}F_{V_F}F_{H_F}(\varepsilon_D/\varepsilon_M)P_A$$

where

$$\begin{aligned}F_\omega&=(N_j+\tfrac{1}{2}\mp\tfrac{1}{2})/\hbar\omega_j\\ F_Q&=|\mathbf{Q}\,.\,\mathbf{e}_j|^2e^{-2w(Q)}\\ F_{k_I}&=1/k_I\\ F_{k_F}&=k_F^3/\tan\theta_A\,.\end{aligned} \qquad (18)$$

This form of the integrated intensity collects the explicit dependence on $\hbar\omega$, Q, k_I, k_F, and horizontal and vertical collimations into separate factors.

To verify these relations, we have carried out a series of measurements using the Brookhaven triple-axis spectrometers. Preliminary measurements were made to determine the reflectivity of the analyzer and the efficiencies of the monitor and detector for the specific elements used in the experiment.

Determination of the reflectivity of the pyrolytic graphite analyzer was carried out using a perfect germanium crystal in the sample position. The 111 reflection of Ge was used to measure P_A for the 002 reflection of the analyzer while the 311 reflection was used to measure the 004 reflectivity. These reflections were chosen to match the sample and analyzer angles as nearly as possible, as well as to remove any higher

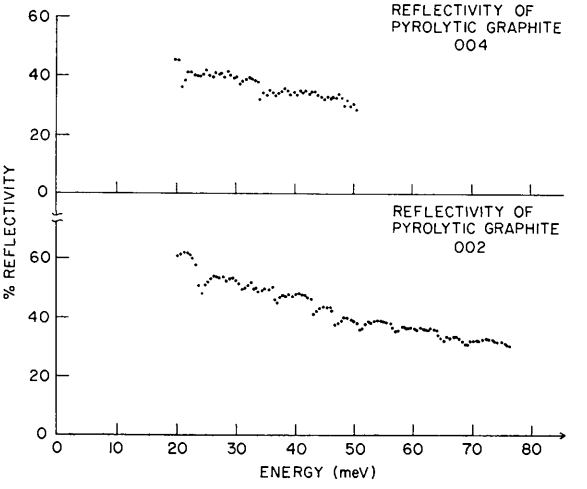

Fig. 3. The reflectivity (P_A) of pyrolytic graphite as a function of energy.

order contamination in the beam. Twenty minute (FWHM) horizontal collimation was used in both positions before the sample. Twenty minute vertical collimation was placed between the sample and the analyzer. The analyzer-to-detector region was left open. The energy was varied by rotating the monochromator, a bent pyrolytic graphite crystal set for the 004 reflection. The reflectivity at a given energy was obtained by taking the ratio of the intensity with the analyzer in position to that with the analyzer removed. The results are shown in Fig. 3. The sharp dips result from competing Bragg reflections as discussed by Shapiro & Chesser (1972).

Determination of $\varepsilon_M/\varepsilon_D$ was then made by moving the monitor to a position directly in front of the detector. Monitor counts *vs.* detector counts were recorded as a function of energy. This ratio differed from the expect $1/V$(V is the velocity of the neutron) only at energies greater than 60 meV. We have assumed therefore that the monitor efficiency is proportional to $1/V$ for all energies and that the detector is black (efficiency = 1·0) for energies less than 60 meV. For energies above that limit, the detector efficiency is given by the deviation of the measured ratio from $1/V$.

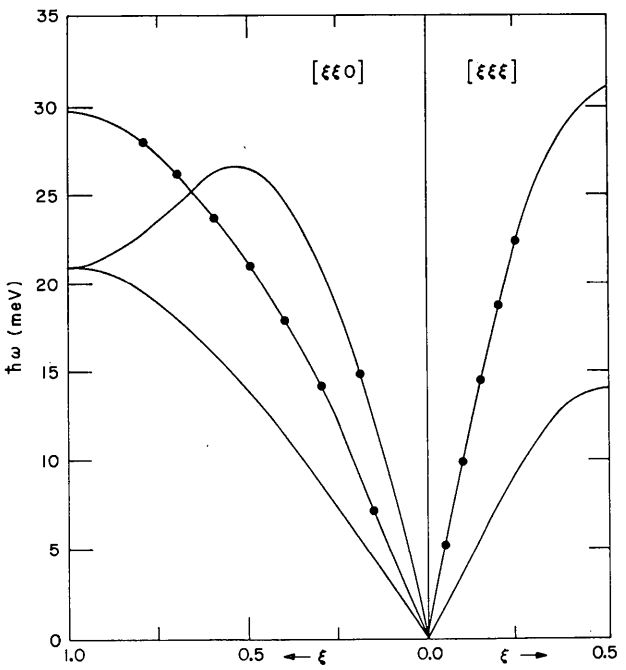

Fig. 4. Phonon dispersion curves for copper at room temperature. Solid lines represent the data of Nicklow *et al.* (1967). Closed circles indicate phonons whose intensities were measured in this study.

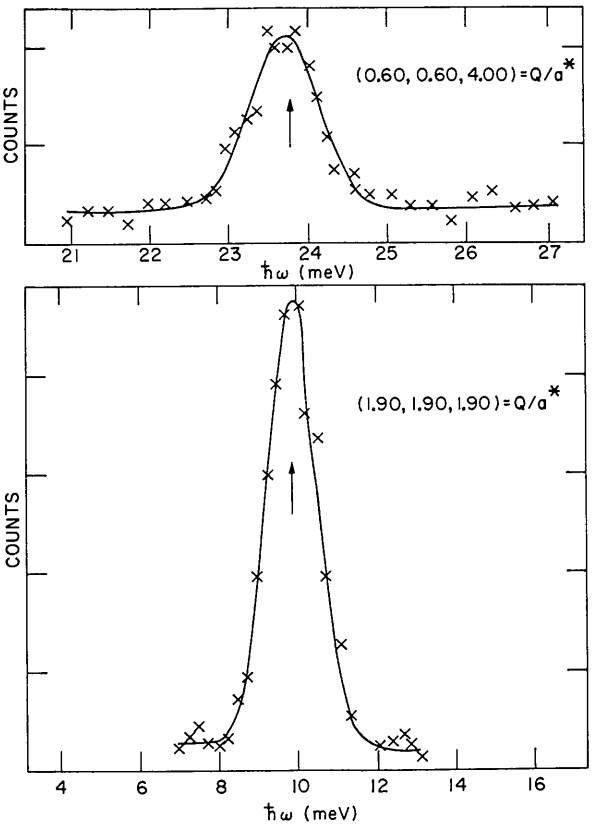

Fig. 5. Typical fits to phonon data for room temperature copper. Solid line is a non-linear least-squares fit to a Gaussian with variable height, width and center, plus background.

The phonon intensity experiments were carried out using a cylindrical sample of copper with mosaic spread of four minutes. The initial energy was selected by a Ge (311) monochromator. The final energy was determined by the pyrolytic graphite analyzer whose reflectivity had been measured earlier. Horizontal

Table 1. *Parameters for sets of scans on a copper sample*

Tested dependence	Q/a^*	E_I(meV)	E_F(meV)	α_2–α_3(minutes)	β_2–β_3(minutes)	Analyzer reflection
Q	Maximally varied	Minimally varied	30	20–20	> 60	002
k_I	Minimally varied	Maximally varied	30	20–20	> 60	002
α	(2·10, 2·10, 2·10)	~40	30	Varied	> 60	002
β	(2·10, 2·10, 2·10)	~40	30	> 60	Varied	002
k_F	Minimally varied	52	Maximally varied	20–20	> 60	002
tan θ_A	Minimally varied	52	Maximally varied	20–20	> 60	004

collimation was twenty minutes (FWHM) throughout, vertical collimation was relaxed. All measurements were carried out at room temperature.

The data were taken so as to form sets of scans in which one parameter was varied over a wide range and the other parameters were confined to as narrow a range as was possible. The parameters of these sets are listed in Table 1. The first sets of measurements were made for phonon creation at a constant final energy of 30 meV. To examine the Q dependence of the integrated intensity, two longitudinal phonons were taken at different values of G, the reciprocal lattice vector. That is ,measurements were made at one value of q, and hence one value of $\hbar\omega$, and several values of Q. Next, several phonons were taken along two branches of the dispersion curve to test the dependence on k_I. These are indicated on the dispersion curves shown in Fig. 4. Using the phonon at $\mathbf{Q}=(2{\cdot}10, 2{\cdot}10, 2{\cdot}10)$ and $\hbar\omega \simeq 10$ meV we measured the intensity for six combinations of horizontal collimation. By turning the Soller collimators after the sample on their sides, we then measured the intensity for six combinations of vertical collimation.

The remaining data were taken at a constant initial energy of 52meV. First, using the 002 reflection of the analyzer, the phonons used to test k_I above were retaken to examine the k_F dependence. Measurements were made for phonon creation and annihilation to increase the range of k_F tested. Then, changing to the 004 reflection of the analyzer, about half of the measurements were repeated to distinguish the dependence on $\tan\theta_A$ as opposed to dependence upon k_F. Each run with varying k_F was corrected point by point for the reflectivity of the analyzer.

The data were then computer-fitted to a Gaussian plus background using a non-linear least-squares program. Typical fits are shown in Fig. 5. The phonon energies, as shown in Fig. 4, are in good agreement with those of Nicklow, Gilat, Smith, Raubenheimer & Wilkinson (1967). The area of the fitted Gaussian was taken to be the measured integrated intensity. Each area for a constant initial energy scan was corrected for detector efficiency appropriate to the final energy at the center of the peak. Each area for a constant-final-energy scan was corrected for monitor efficiency appropriate to the initial energy at the center of the peak.

The value of the constant C_0 was determined by normalizing one standard phonon in each set of runs to the value given by equation (22). Each measured area was then divided by the value predicted by that expression. The results of that division, I_{obs}/I_{calc}, are shown as a function of phonon energy in Fig. 6. On the average, the observed value is within 10% of the calculated integrated intensity. This is consistent with the experimental uncertainties in the measured intensities as determined by the fitting program. Bearing in mind that the raw data vary by as much as a factor of 50, the agreement in Fig. 6 is quite good. We have taken the lack of systematic deviation in that figure to indicate that the dependence on $\hbar\omega$ is as predicted.

Fig. 7 shows the dependence on Q for longitudinal phonons. The Debye–Waller factor for room temperature copper is taken to be

$$W(Q)=(0{\cdot}0105)\times(Q/a^*)^2$$
$$a^*=1{\cdot}741\ \text{Å}^{-1} \qquad (19)$$

as computed from the measurements of Owen & Williams (1947). Fig. 8 shows the explicit dependence on k_I for two branches of the dispersion curve. The scatter in these two figures is within reasonable limits and verifies the expected dependence on Q and on k_I. A least-squares fit to the exponent of k_I for the data in

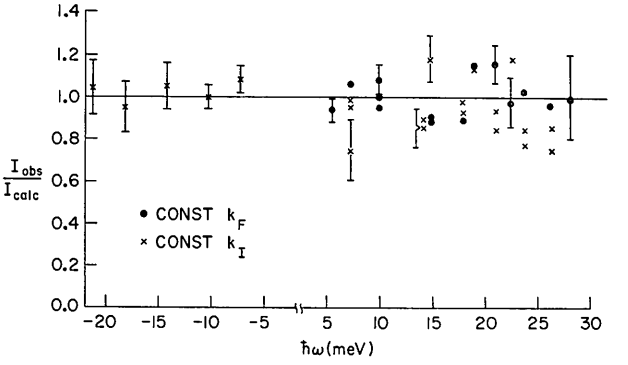

Fig. 6. Ratio of observed to calculated integrated intensities as a function of $\hbar\omega$. Data for variation in Q, k_I and k_F is indclued.

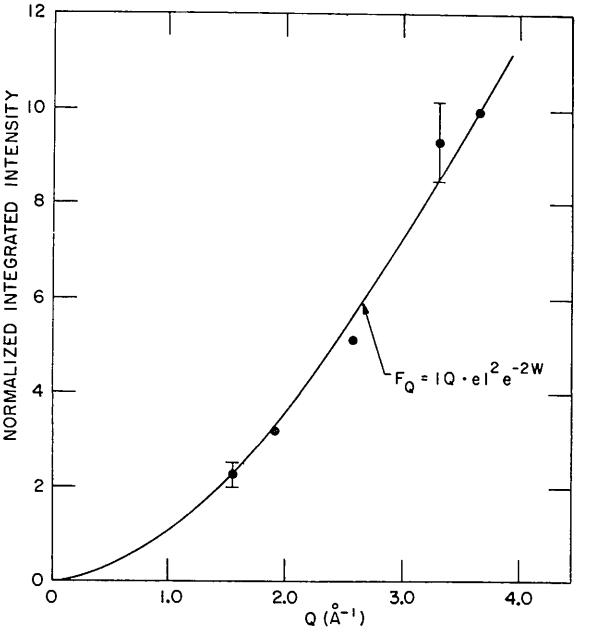

Fig. 7. Integrated intensities as a function of Q, corrected for $\hbar\omega$ and k_I and normalized at $3{\cdot}6\ \text{Å}^{-1}$. Only longitudinal phonons are included.

Fig. 8 gives a value of $-0{\cdot}9 \pm 0{\cdot}3$. Thus the dependence on Q and k_I is verified.

Figs. 9 and 10 show the dependence on horizontal and vertical collimation respectively. As is shown by the dashed curves, it is important to consider the blocking effect due to the finite thickness of the collimator vanes. This effect is discussed in detail by Rossitto & Poletti (1971).

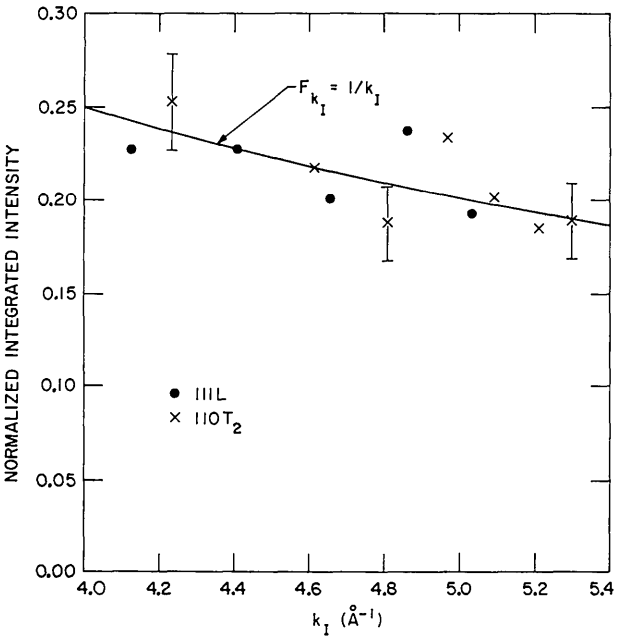

Fig. 8. Integrated intensities as a function of k_I, corrected for Q and $\hbar\omega$. Separate normalizations for the (111)L and (110)T_2 branches (at 4·4 Å^{-1} and 4·6 Å^{-1}) were required in this case due to intervening physical modifications to the spectrometer.

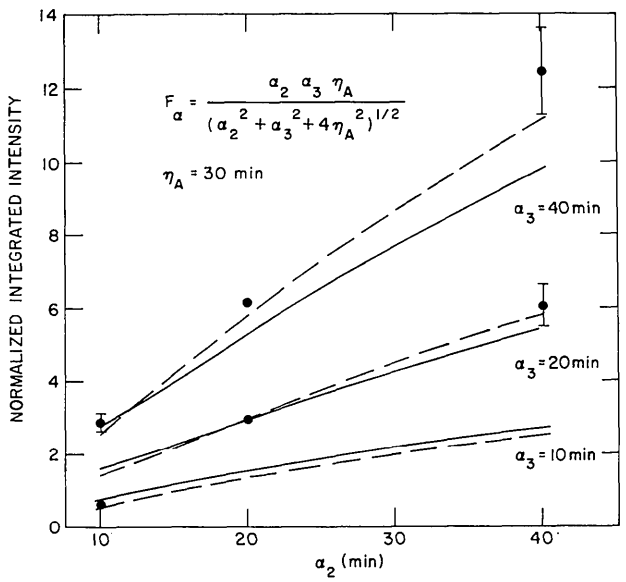

Fig. 9. Integrated intensities as a function of horizontal collimation, normalized so that the point at 20 min–20 min lies on the curve. The solid lines are F_α alone while the dashed curves also include the blocking effect due to the finite thickness of the collimator vanes.

Fig. 11 shows the results of the measurements carried out at a constant initial energy. The dependence of the integrated intensity on k_F and on $\tan\theta_A$ is adequately verified. The consistency of these data gives added confidence to the method used to correct for analyzer reflectivity and for detector efficiency.

The expression derived above for the measured integrated intensity has been verified and can be used to correct data for resolution effects. If the collimation is unchanged within an experiment, a single normalization should suffice for all data. Whenever the collimation after the sample is changed, however, a normalization check would seem to be good procedure since the variation with those parameters is not completely explained. The difficulty can sometimes be avoided by changing the collimation before the monitor since the monitor will perform the normalization automatically.

Comparison of constant initial energy data to constant final energy scans suggests a slight advantage in favor of constant final energy (an average error of 7% as opposed to 11% for constant initial energy). There is also the obvious experimental advantage that the monitor automatically removes the k_I dependence and that no measurement of analyzer reflectivity need be performed. Care must be taken, however, to remove higher-order contamination before the monitor since the extent of this contamination will vary with energy. It must be noted that many spectrometers are not equipped to vary k_I. This experiment proves that this restriction does not prohibit measurements of integrated intensities.

We would like to thank Professor Robert Nathans for a critical reading of the manuscript. We would also like to thank Dr F. W. Young Jr and Dr R. M. Nicklow at Oak Ridge National Laboratory for the excellent copper crystal. We are grateful for many beneficial discussions with our colleagues, particularly Dr G. Shirane and Dr J. Skalyo Jr.

APPENDIX

It should be noted that there are several typographical errors in the references used. The following should be corrected to read:

Cooper & Nathans (1967)

$$a_{11}^2 = [(4\sin^2\theta_M \eta_M'^2 + \beta_0^2)^{-1} + (\beta_1^2)^{-1}]k_I^{-2} \qquad (55a)$$

$$a_{12}^2 = [(4\sin^2\theta_A \eta_A'^2 + \beta_3^2)^{-1} + (\beta_2^2)^{-1}]k_F^{-2}\,. \qquad (55b)$$

$$I_W = R_0 2\pi R_{33}\sqrt{G_1 G_2}\,\exp\{-\tfrac{1}{2}G_3^2 W^2\} \qquad (66)$$

$$G_3^2 = M_{44} - G_1(M_{14} - C_1 M_{44})^2 - G_2(C_2 M_{44} - M_{24} + G_1[M_{14} - C_1 M_{44}] \times [M_{12} - C_1 M_{24} - C_2 M_{14} + C_1 C_2 M_{44}])^2 . \quad (67d)$$

Tucciarone, Lau, Corliss, Delapalme & Hastings (1971)

$$D_0 = \frac{\pi \varepsilon P_M P_A}{2 \sin\theta_M \sin\theta_A} \left(\frac{1}{\beta_0^2} + \frac{1}{4\sin^2\theta_M \eta_M'^2}\right)^{-1/2} \times \left(\frac{1}{\beta_3^2} + \frac{1}{4\sin^2\theta_A \eta_A'^2}\right)^{-1/2} \times 2\pi k_I \cot\theta_M \left[\left(\frac{1}{\eta_M^2} + \frac{4}{\alpha_0^2}\right)\left(\frac{1}{\eta_M^2} + \frac{1}{\alpha_0^2} + \frac{1}{\alpha_1^2}\right) - \left(\frac{1}{\eta_M^2} + \frac{2}{\alpha_0^2}\right)^2\right]^{-1/2} \times 2\pi k_F \cot\theta_A \left[\left(\frac{1}{\eta_A^2} + \frac{4}{\alpha_3^2}\right)\left(\frac{1}{\eta_A^2} + \frac{1}{\alpha_3^2} + \frac{1}{\alpha_2^2}\right) - \left(\frac{1}{\eta_A^2} + \frac{2}{\alpha_3^2}\right)^2\right]^{-1/2} \times 2\pi \left[\frac{1}{4\sin^2\theta_M \eta_M'^2 + \beta_0^2} + \frac{1}{\beta_1^2}\right]^{-1/2} \times \left[\frac{1}{4\sin^2\theta_A \eta_A'^2 + \beta_3^2} + \frac{1}{\beta_2^2}\right]^{-1/2} . \quad (5\cdot10)$$

$$\Delta V = (2\pi)^3 k_I^2 k_F^3 \sin(2\theta_S) A'^{1/2} \frac{(a_{11}^2 + a_{12}^2)^{1/2}}{a_{11} a_{12}} \times \cot\theta_M \left[\left(\frac{1}{\eta_M^2} + \frac{4}{\alpha_0^2}\right)\left(\frac{1}{\eta_M^2} + \frac{1}{\alpha_0^2} + \frac{1}{\alpha_1^2}\right) - \left(\frac{1}{\eta_M^2} + \frac{2}{\alpha_0^2}\right)^2\right]^{-1/2} \times \cot\theta_A \left[\left(\frac{1}{\eta_A^2} + \frac{4}{\alpha_3^2}\right)\left(\frac{1}{\eta_A^2} + \frac{1}{\alpha_3^2} + \frac{1}{\alpha_2^2}\right) - \left(\frac{1}{\eta_A^2} + \frac{2}{\alpha_3^2}\right)^2\right]^{-1/2} . \quad (5\cdot12)$$

These are in addition to the error noted in § 2.

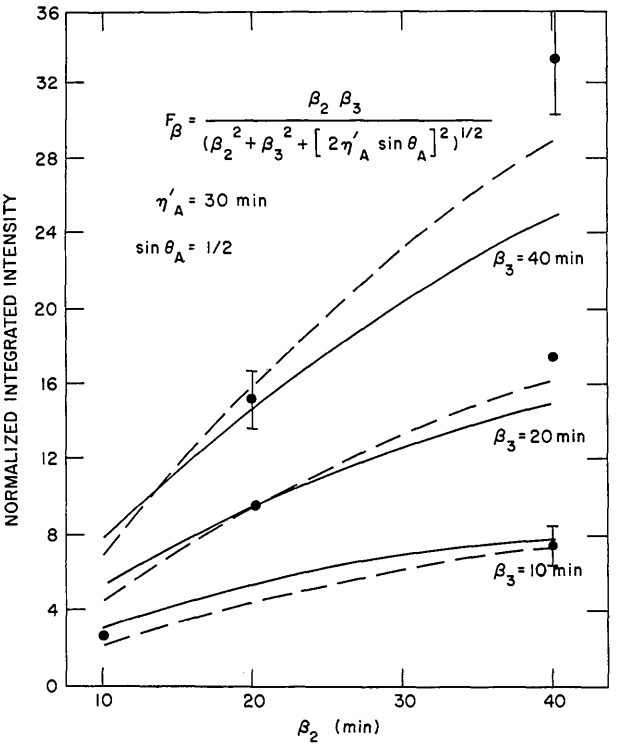

Fig. 10. Integrated intensities as a function of vertical collimation, normalized so that the point at 20 min–20 min lies on the curve. The solid lines are F_β alone while the dashed curves include the blocking effect discussed above.

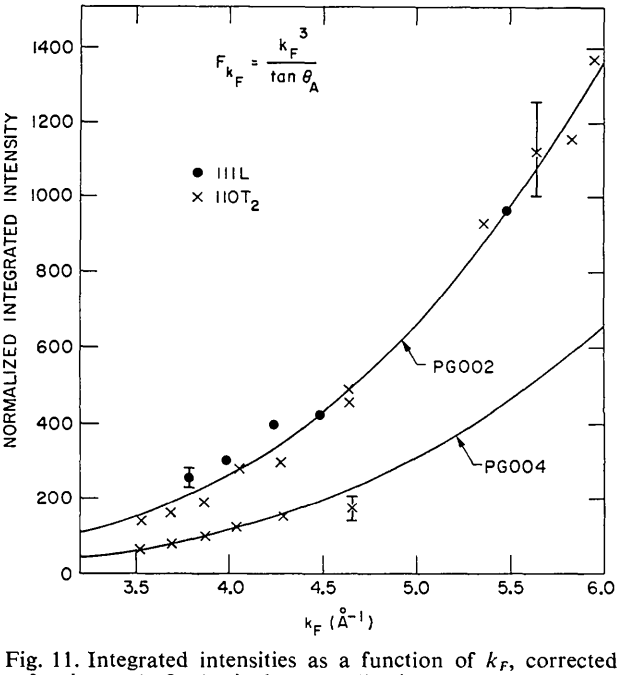

Fig. 11. Integrated intensities as a function of k_F, corrected for $\hbar\omega$ and Q. A single normalization was employed at 4·5 Å^{-1}. Two analyzers were used to distinguish dependence on θ_A from dependence on k_F.

References

Bjerrum Møller, H. & Nielsen, M. (1970). *Instrumentation for Neutron Inelastic Scattering Research* p. 49–76. Vienna: IAEA.

Caglioti, G., Paoletti, A., & Ricci, F. P. (1958). *Nucl. Instrum. Meth.* **3**, 223–228.

Collins, M. F. (1963). *Brit. J. Appl. Phys.* **14**, 805–809.

Cooper, M. J. & Nathans, R. (1967). *Acta Cryst.* **23**, 357–367.

Dorner, B. (1972). *Acta Cryst.* A**28**, 319–327.

NICKLOW, R. M., GILAT, G., SMITH, H. G., RAUBENHEIMER, L. J. & WILKINSON, M. K. (1967). *Phys. Rev.* **164**, 922–928.
NIELSEN, M. & BJERRUM MØLLER, H. (1969). *Acta Cryst.* A**25**, 547–530.
OWEN, E. A. & WILLIAMS, R. W. (1947). *Proc. Roy. Soc.* A**188**, 509–511.
ROSSITTO, F. & POLETTI, G. (1971). *Acta Cryst.* A**27**, 341–347.
SAMUELSEN, E. J., HUTCHINGS, M. T. & SHIRANE, G. (1970). *Physica*, **48**, 13–42.
SEARS, V. F. & DOLLING, G. (1972). AECL Report No. 4133.
SHAPIRO, S. M. & CHESSER, N. J. (1972). *Nucl. Instrum. Meth.* **101**, 183–186.
STEDMAN, R. (1968). *Rev. Sci. Instrum.* **39**, 878–883.
STEDMAN, R. & NILSSON, G. (1966). *Phys. Rev.* **145**, 492–500.
TUCCIARONE, A., LAU, H. Y., CORLISS, L. M., DELPALME, A. & HASTINGS, J. M. (1971). *Phys. Rev.* B**4**, 3206–3245.
WERNER, S. A. & PYNN, R. (1971). *J. Appl. Phys.* **42**, 4736–4749.

Acta Cryst. (1973). A**29**, 171

Coincidence-Site Lattices

BY A. SANTORO AND A. D. MIGHELL

Institute for Materials Research, National Bureau of Standards, Washington, D.C. 20234, *U.S.A.*

(*Received* 19 *July* 1972; *accepted* 27 *September* 1972)

Coincidence-site lattices are characterized mathematically, in the general case, by a method that can be applied to a pair of original lattices of any symmetry, either metrically identical or metrically different, does not involve inspection and is readily adaptable to computer calculations. The procedure is illustrated by several numerical examples. The proposed characterization of coincidence-site lattices is based on the theory of derivative lattices and makes extensive use of the concepts of superlattice and sublattice. Appended is a simple procedure for determining the transformation matrices needed to generate superlattices and sublattices of any multiplicity.

Introduction

In recent years field-ion and electron-microscopy studies have shown that, in many materials of metallurgical interest, the two crystals forming a grain boundary are often mutually oriented so that they have a common superlattice which continues without disturbance from one crystal to the other. This superlattice is called *coincidence-site lattice* and the two crystals adjacent to the boundary are said to be in a *coincidence-site relationship or coincidence-site related.* The occurrence and importance of coincidence-site lattices was first pointed out by Kromberg & Wilson (1949) in their study on secondary recrystallization of copper. Since then the concept of coincidence-site lattice has been used in the study of the 'structure' of grain boundaries (Brandon, Ralph, Ranganathan & Wald, 1964; Brandon, 1966; Morgan & Ralph, 1967) and in connection with such subjects as grain-boundary migration in high-purity materials (Aust & Rutter, 1959) and nucleation and growth of boundary precipitates (Unwin & Nicholson, 1969).

The interpretation of experimental results in terms of the coincidence-site lattice model requires the knowledge of the geometrical conditions under which two crystals are coincidence-site related. The problem of characterizing mathematically two identical lattices of any symmetry and randomly oriented with respect to each other has been treated by Goux (1961) and Lange (1967). Ranganathan (1966) has given a method for determining the axis and the angle of the rotation necessary to bring two identical cubic lattices, initially coincident, into a coincidence-site relationship and Ranganathan (1967) and Acton & Bevis (1971) have presented comprehensive tables of the angle–axis pairs for the cubic system. The proposed procedure involves several stages of inspection and can only be applied to cubic crystals of the same species.

The mathematical characterization of a coincidence-site lattice of any symmetry and for lattices differing metrically as well as in orientation, may be useful in the analysis of a great variety of grain boundaries and in the study of regular aggregates such as twins and epitaxic and syntaxic intergrowths. As part of a systematic study of the geometrical properties of lattices, a method for the determination of coincidence-site lattices in the general case has been derived. It is essentially an application of the theory of derivative lattices, and its use requires the systematic derivation of superlattices and sublattices of any multiplicity. This derivation can be made either by means of the procedure proposed by Santoro & Mighell (1972) or, more simply, by means of the method presented in the Appendix to this paper.

General

Two lattices Λ' and Λ'' can be coincidence-site related if, and only if, two superlattices, Γ' derived from Λ'